energies

MDPI

Article

The Potential of Activated Carbon Made of Agro-Industrial Residues in NO_x Immissions Abatement

Imen Ghouma [1,2], Mejdi Jeguirim [1,*], Uta Sager [3], Lionel Limousy [1], Simona Bennici [1], Eckhard Däuber [3], Christof Asbach [3], Roman Ligotski [4], Frank Schmidt [4] and Abdelmottaleb Ouederni [2]

1 Institut de Sciences des Matériaux de Mulhouse, Université de Haute-Alsace, 15 Rue Jean Starcky, F-68057 Mulhouse, France; imenghouma83@gmail.com (I.G.); lionel.limousy@uha.fr (L.L.); simona.bennici@uha.fr (S.B.)

2 Department of Chemical Engineering, National School of Engineers (ENIG), University of Gabes, Avenue Omar Ibn El Khattab, Gabes 6029, Tunisia; mottaleb.ouederni@enig.rnu.tn

3 Institut für Energie-und Umwelttechnik e.V., Bliersheimer Str. 58-60, D-47229 Duisburg, Germany; sager@iuta.de (U.S.); daeuber@iuta.de (E.D.); asbach@iuta.de (C.A.)

4 Nanopartikel Prozesstechnik, Universität Duisburg-Essen, Lotharstr. 1, D-47057 Duisburg, Germany; roman.ligotski@uni-due.de (R.L.); frank.schmidt@uni-duisburg.de (F.S.)

* Correspondence: mejdi.jeguirim@uha.fr; Tel.: +33-389-608-661

Received: 22 June 2017; Accepted: 25 September 2017; Published: 28 September 2017

Abstract: The treatment of NO_x from automotive gas exhaust has been widely studied, however the presence of low concentrations of NO_x in confined areas is still under investigation. As an example, the concentration of NO_2 can approximate 0.15 ppmv inside vehicles when people are driving on highways. This interior pollution becomes an environmental problem and a health problem. In the present work, the abatement of NO_2 immission is studied at room temperature. Three activated carbons (ACs) prepared by physical (CO_2 or H_2O) or chemical activation (H_3PO_4) are tested as adsorbents. The novelty of this work consists in studying the adsorption of NO_2 at low concentrations that approach real life immission concentrations and is experimentally realizable. The ACs present different structural and textural properties as well as functional surface groups, which induce different affinities with NO_2. The AC prepared using water vapor activation presents the best adsorption capacity, which may originate from a more basic surface. The presence of a mesoporosity may also influence the diffusion of NO_2 inside the carbon matrix. The high reduction activity of the AC prepared from H_3PO_4 activation is explained by the important concentration of acidic groups on its surface.

Keywords: activated carbon; NO_2 adsorption; ambient temperature; low NO_2 concentrations; textural properties-surface chemistry characterization

1. Introduction

The increase of the threatening substances emission to the atmosphere has become a major environmental problem. Among the various harmful gases, nitrogen oxides (NO_x) have a negative impact through the smog and acid rain formations as well as the decrease of the superior ozone layer [1,2]. Several methods have been applied for nitrogen oxides elimination including the reduction of NO_x by selective non-catalytic reduction (SNCR) and selective catalytic reduction (SCR) [3]. However, these techniques have several drawbacks such as costs and technical complexity. Therefore, the separation by adsorption at reduced temperatures is receiving increasing attention. Several adsorbents including zeolites, perovskites and carbonaceous materials were tested for NO_x

treatment [4–6]. However, studies on activated carbons (AC) performance for NO_x removal showed promising results in term of adsorption efficiencies [7–12].

Several lignocellulosic precursors were used for the preparation of activated carbons dedicated to the NO_2 removal at ambient temperature [7–12]. These carbonaceous adsorbents showed interesting adsorption capacities ranging between 40 mg/g and 120 mg/g. However, the performance of these activated carbons was generally evaluated at 500–1000 ppm NO_2 concentrations in presence of air under dry and wet conditions. These experimental conditions are far from the ones encountered at ambient air especially near urban traffics and industrial plants.

Despite the emission reduction measures implemented for automotive and industrial exhaust gases [13–16], vehicle occupants and urban population are particularly affected by high or even increasing nitrogen oxides immissions. As a result, the interest in adsorptive cabin air filters and HVAC (Heating, Ventilation and Air Conditioning) filters is rising. This interest leads to more research on the adsorptive separation of low concentrations of nitrogen oxides at ambient temperatures. In this context, Sager et al. have examined the performance of different activated carbons in cabin air filter for the elimination of several pollutants [17–21]. In particular, authors examined the adsorption of low concentrations of NO_2 on modified activated carbon, prepared of polymer as base material, at ambient temperatures. They have showed that the elimination of NO_2 present in the air, on activated carbons at ambient temperature, and after repeated adsorption cycles, can be increased by the infiltration of metal oxide nanoparticles into the sorbent. In this case the regeneration of the filter was assumed to be connected to the redox properties of the sorbent that can act also as reduction catalyst towards NO_x [18–21]. However, the role of surface chemistry of the activated carbon on the NO_2 adsorption/reduction was not examined in detail.

Due to industrial activities and the urban traffic, NO_x emissions are also a problem in developing countries such as Tunisia that has few resources and is rather agricultural and agro-industrial outside the urban agglomerations. One approach to counteract both problems is the development of an efficient sorbent for the separation of NO_x from a locally available raw precursor; in this case, the agro-industrial residue olive stones have interesting potential for activated carbons preparation [22]. Ghouma et al. [10] have prepared activated carbon based on olive stones by water vapor activation. The adsorption tests with 500 ppm NO_2 have shown that the prepared activated carbon has a capacity as high as the ones available in literature. Furthermore, it was demonstrated that, besides microporosity, the surface functional groups are strongly related to the NO_2 adsorption capacity. However, the investigation of the AC performance at low concentrations as well as the determination of the precise contribution of the different activated carbon characteristics to NO_2 adsorption performance are still missing.

Based on the described considerations and experience, a study was started with regard to which extent the potential of activated carbon from olive stones can be enhanced by the different activation methods resulting in modifications of the functional groups on the inner surface and surface characteristics.

For that purpose, three differently activated carbons prepared from olive stones were evaluated with breakthrough tests using NO_2 (5 ppmv as inlet concentration) as the adsorptive at ambient temperature and 50% of relative humidity (RH). Two activated carbons were prepared by gas phase activation. A first sample was prepared by water vapor treatment, while a second was activated with carbon dioxide (CO_2). A third activated carbon was prepared by chemical activation with phosphoric acid (H_3PO_4). The differently activated sorbents were characterized with regard to their pore structure, morphology and carbon surface chemistry using nitrogen adsorption, scanning electron microscopy, Fourier transform infrared spectroscopy, and temperature-programmed desorption coupled with mass-spectrometry. The results of the breakthrough tests were correlated to the results of AC characterization with the aim to identify the key-parameters influencing the adsorption capacity, and then to adjust the carbon activation and modification methods to obtain better performing sorbents.

2. Materials and Methods

2.1. Samples Preparation

Carbon materials were prepared from olive pomace provided by a Tunisian olive oil factory located in Zarzis. The raw precursor was washed abundantly with hot distilled water and dried at ambient temperature for 24 h. Then, the dried olive stones were crushed and sieved to 1–3 mm particle size. Different activated carbons were prepared through chemical and physical activations of olive stones according to the following protocols.

2.1.1. Chemical Activation

A granular H_3PO_4-activated sample was prepared according to the optimized protocol reported by Limousy et al. [22]. Briefly, olive stones were soaked in an aqueous solution of orthophosphoric acid (50%, *w*/*w*) at the weight ratio (1:3). The suspension was stirred at 110 °C for 9 h. Then, the filtered material was dried and carbonized in nitrogen flow at 170 °C for 30 min and finally at 410 °C for 2 h 30 min. The resulting carbon, denoted as AC-H_3PO_4, was then washed abundantly with distilled water until the elimination of all acid traces, and was dried overnight at 110 °C. The yield of chemical activation method was 33 wt %. Referring to the recent work published on chemically activated carbon, it is shown that this yield is more important that KOH activation of biomass. Travis et al. [23] have synthesized a series of KOH activated carbons from spent coffee grounds. Sample yields ranged from 11 to 16 wt % with yields lower for higher KOH.

2.1.2. Physical Activation

The carbonization and the activation steps were carried out in a fixed bed reactor in a stainless steel reactor placed in a vertical automated furnace equipped with a temperature controller, with an initial mass of biomass equal to 2 g. Firstly, the precursor was carbonized under nitrogen flow at 600 °C for 2 h. Subsequently, the activation of the resultant char was performed by switching the gas either to pure CO_2 or to water vapor. The targeted temperature was maintained to 750 °C for 6 h. Further details about physical activation procedure could be found in a previous work [10].

2.2. Characterization of Activated Carbons

2.2.1. Pore Structure and Morphology Characterization

Characterization of the pore structure of the activated carbon samples was made by measurement of N_2 adsorption isotherms using an automatic gas sorption analyzer (ASAP 2010, Micrometrics). Specific surface area was calculated from the N_2 adsorption isotherms applying the Brunauer–Emmett–Teller (BET) equation and yield important information about structural features. The total pore volume was determined from the amount of nitrogen adsorbed at $P/P^\circ = 0.99$. The t-plot method was applied to measure the total micropore volume.

Scanning electron microscopy (Philips model FEI model Quanta 400 SEM) was used to analyze morphology of the different activated carbons.

2.2.2. Characterization of Carbon Surface Chemistry and Composition

Temperature Programmed Desorption Coupled with Mass Spectrometry (TPD-MS)

The surface chemistry of samples was analyzed by TPD-MS. The sample weighting 10 mg was placed in quartz tube in an oven and heat-treated with a linear heating rate of 5 °C/min under vacuum. The material surface chemistry was evaluated in the temperature range 25–900 °C. The gases evolved during the heating process were continuously analyzed quantitatively by a mass spectrometer (INFICON Transpector). The desorption rate of each gas as a function of temperature was determined

from the TPD analysis. The total amount of each gas released was computed by time integration of the TPD curves.

Fourier Transform Infrared Spectroscopy (FTIR)

FTIR was used to characterize the main functional groups of the activated carbon surface using a spectrometer FTIR (Jasco FT-IR 4100 series spectrophotometer with a diffuse reflectance accessory manufactured by PIKE Technologies, Madison, WI, USA). During this characterization, samples of activated carbon were mixed with finely divided spectroscopic grade KBr. All the spectra were taken at a spectral resolution of 16 cm^{-1} using minimum 30 scans.

2.3. NO_2 Adsorption Experiments

The different sorbents were tested by breakthrough experiments in a test set-up with a fixed-bed flow reactor with an inner diameter of 0.05 m (see Figure 1). In each test, 2 g of activated carbon was packed in the breakthrough column with a resulting bed length of about 2.5 mm. The very low bed length should represent the ultrathin sorbent layers of commercially available cabin air filters and filters for heating, ventilation and air conditioning purposes used for the reduction of ambient pollution. Then, an air stream of 23 °C and 50% relative humidity with 5 ppm_V NO_2 was forced to pass through the sorbent layer with a velocity of 0.2 m/s. The NO_2 was directly supplied to the airflow from a reservoir using a mass flow controller. To avoid condensation and to achieve the required vapor pressure, the NO_2 reservoir, the tubing, and the mass flow controller were heated and kept at about 35 °C. At the inlet and outlet of the fixed-bed reactor, the concentrations of NO_2 and NO were measured with two nitrogen oxide analyzers (type AC 31M from Ansyco, Karlsruhe, Germany) using chemiluminescence. The measuring range of the analyzers is up to 10 ppmv and the lower detection limit is <1 ppb. As the precision of the measurement is ±1% of the upper range value at input concentrations of 5 ppm_V, the measurement uncertainty causes a lack of significance of breakthrough values below 2%. In the test rig the total pressure corresponds approximately to the atmospheric pressure. Before the tests, the activated carbon samples were conditioned in air stream at 23 °C and 50% relative humidity, for 15 min.

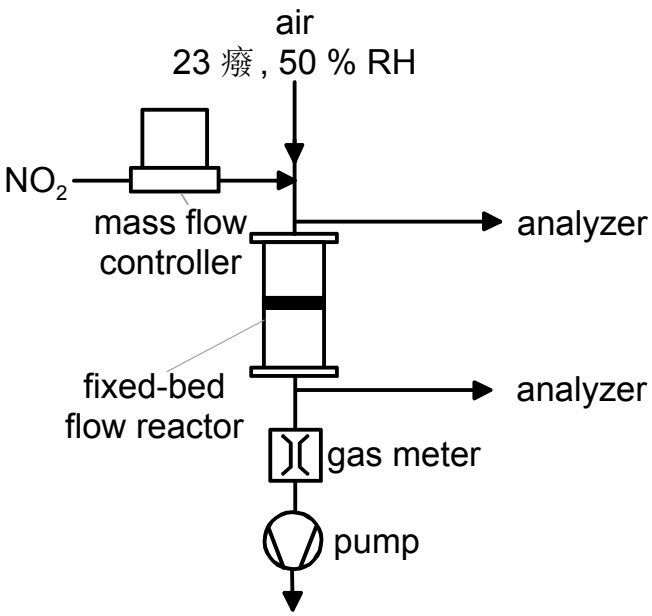

Figure 1. Sketch of the test device for breakthrough experiments.

3. Results and Discussion

3.1. Activated Carbon Characterization

3.1.1. Morphology and Pore Structure Characterizations

Scanning electron microscopy (SEM) micrographs of AC-H_3PO_4, AC-CO_2 and AC-H_2O are gathered in Figure 2. The three samples have shown remarkable differences in the surface morphology, thus revealing different activation mechanisms. The sample AC-H_3PO_4 was arranged in tightly compacted sheets (see Figure 2a). Actually, the phosphoric acid acts as an acid catalyst to promote bond cleavage and formation of cross-links via cyclization/condensation reactions. The deposited H_3PO_4 can react with organic species to form phosphate and polyphosphate bridges that connect and cross-link biopolymer fragments. The addition (or insertion) of phosphate groups drives a process of dilation that, after the removal of the acid, leaves the matrix in an expanded state characterized by an accessible pore structure [24]. Similar observations were observed during chemical activation. As an example, KOH reacts with carbon to yield carbonates/bicarbonates at intermediate temperatures and further increase in the temperature leads to the decomposition and gasification to create porosities [25,26]. In addition, during ZnO chemical activation, different reduction reactions occur to generate high porosities.

The physically activated carbons AC-CO_2 and AC-H_2O show quite similar surface morphologies. Figure 2b,c shows irregular shaped particles with large concoidal cavities and smooth surfaces for both activated carbons.

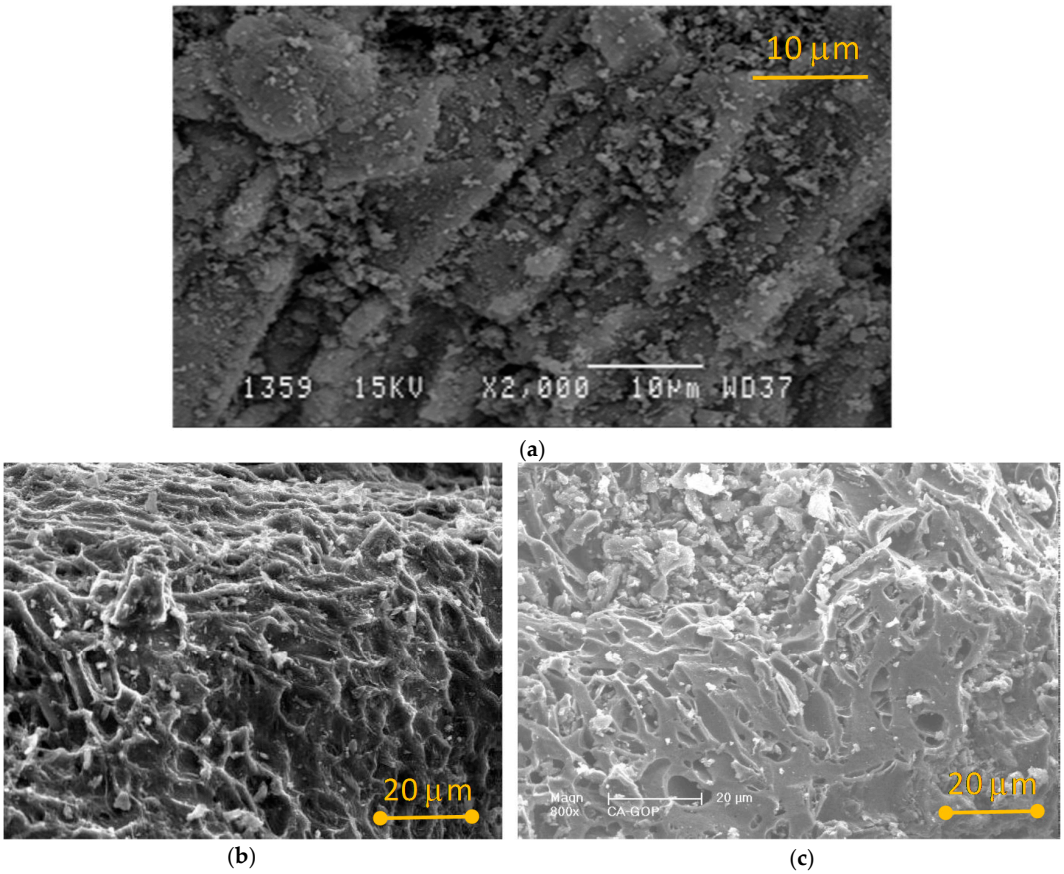

Figure 2. Scanning electron microscopy micrographs of sample: (**a**) AC-H_3PO_4; (**b**) AC-CO_2; and (**c**) AC-H_2O.

Figure 3a shows the nitrogen adsorption isotherms measured at −196 °C for the prepared carbon materials. All the ACs show Type-I isotherm according to the IUPAC classification except the isotherm

related to the sample AC-H_2O which is typically of Type III. Therefore, all carbons are basically microporous. In addition, AC-H_2O exhibits mesopores in its internal structure. Such results were also observed by Roman et al. during the preparation of activated carbons from almond tree pruning through water vapor activation [27]. This results clearly indicates that the physical activation modes are different for H_2O and CO_2. Water vapor tends to react faster than carbon dioxide which leads to the formation of a highly mesoporous activated carbon. Such behavior for water vapor is due to the burning or also called as gasification of more carbon source at the given temperature, in the form of CO_2 ($C + H_2O \rightarrow CO/CO_2 + H_2$). At the opposite, carbon dioxide generates only micropores. This may be due to both the difference of reactivity of these two molecules but also to the difference of diffusion coefficients [28]. Moreover, the AC-H_3PO_4 carbon shows the highest nitrogen uptake at −196 °C, thus displaying the highest surface area and the best-developed porosity. Such an observation is confirmed by the pore size distribution shown in Figure 3b. In fact, Figure 3b shows for AC-H_3PO_4 only the presence of micropores (size < 2 nm) with high micropores volume comparing to AC-CO_2. In contrast, AC-H_2O exhibits a large size range of mesoporosity created by water vapor activation. The textural properties of the carbon materials deduced from adsorption isotherms of N_2 at −196 °C are compiled in Table 1.

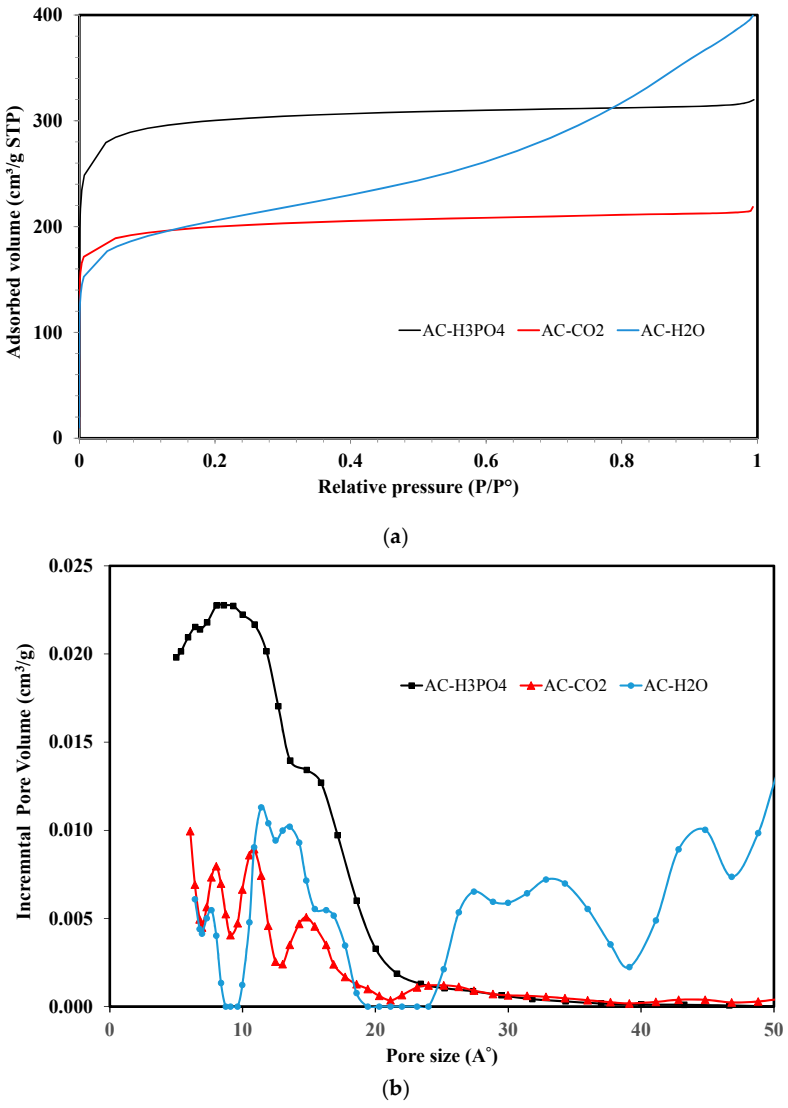

Figure 3. (**a**) Nitrogen adsorption/desorption isotherm of the different activated carbons; and (**b**) density functional theory (DFT) pore size distribution.

Table 1. Textural parameters of the activated carbons.

Carbons	S_{BET} (m^2/g)	S_{ext} (m^2/g)	S_{μ} (m^2/g)	$V_{T\ pore}$ (cm^3/g)	V_{micro} (cm^3/g)	V_{meso} (cm^3/g)	% micro	D_p (A)
AC-H3PO4	1178	11	1167	0.49	0.45	0.04	92	16.7
AC-CO2	757	83	674	0.32	0.30	0.02	94	17.5
AC-H2O	754	291	463	0.58	0.28	0.30	48	32.2

% micro = $(V_{micro}/V_{Tpore}) \times 100$, D_p: average pore diameter.

3.1.2. Characterization of Carbon Surface Chemistry

TPD-MS experiments give the evolution of CO_2 and CO emissions, as a result of the decomposition of the oxygen functionalities existing at the surface of the activated carbons. The determination of the amount of CO and CO_2 evolved gives an estimation of the amount of surface oxygen groups on the activated carbons. Moreover, the analysis of these emissions according to temperature indicates the presence of different oxygen surface groups.

The analysis of the desorption rates of CO_2 indicates the presence of different surface oxygen groups. In particular, the emission of CO_2 below 400 °C indicate the presence of carboxylic groups at the surface of the different activated carbons [29]. However, AC-CO_2 curve shows a CO_2 emission peak at 520 °C attributed to lactone group decomposition. In contrast, AC-H_3PO_4 and AC-H_2O curves present CO_2 peaks at higher temperature (see Figure 4a) accompanied by CO emission (see Figure 4b). This decomposition indicates the presence of anhydride groups for the AC-H_3PO_4 and AC-H_2O samples.

In a similar way, the analysis of the CO desorption rates shows the higher amount of surface oxygen groups for the AC-H_3PO_4. The CO decomposition could be attributed to carbonyl, quinone, ether and phenol groups. For the physically activated carbons, the CO peaks are obtained at different temperatures. Hence, the CO peak was obtained at 700 °C for the AC-H_2O attributed to phenol group decomposition. In contrast, the CO peak for AC-CO_2 is obtained at 830 °C attributed to quinone groups.

The cumulated amounts of the emitted gases during TPD-MS are shown in Table 2. A significant amount of emitted hydrogen is observed for AC-H_2O. Such emission may be attributed to water vapor activations, which leads to a higher hydrogenation of the carbon surface due to the water gas shift reaction (production of CO_2 and H_2 at the surface of the AC).

The infrared spectra of the different activated carbons are shown in Figure 5. For the spectrum of AC-H_2O, the presence of a broad band located between 3020 and 3300 cm^{-1} is observed. This band corresponds to the aromatic C-H groups. This band is related to the formation of the microcrystalline structure of this activated carbon. A second band between 1100 cm^{-1} and 1300 cm^{-1} assigned to the C-O groups present in the aromatic rings. The presence of a peak located at about 879 cm^{-1} is also observed, which is attributed to the aliphatic C-H elongation. Another peak located at around 1462 cm^{-1} is attributed to the elongation of the aromatic group. On the other hand, this spectrum shows the absence of significant peaks for the bands corresponding to the OH, C=O groups and the C-O-C groups. This behavior suggests that this activated carbon is primarily an aromatic polymer.

For the spectrum of AC-CO_2, the presence of an intense peak attributed to the hydroxyl groups located at 3140 cm^{-1} is noted. Reddy et al. reported the same observations in their comparative study of the two activated carbons prepared from date palm cores activated by CO_2 and H_3PO_4 [30]. For the activated carbon AC-H_3PO_4, a broad and intense shoulder between 3000 and 3500 cm^{-1} was observed. It was associated to the stretching vibrations of hydroxyl groups involved in hydrogen bonding [31]. The band at 1700–1710 cm^{-1} is generally ascribed to the stretching vibrations of C=O bond in carboxylic acid and lactone groups. However, the peak at 1600 cm^{-1} is attributed to a quinone structure. The band at 1250 cm^{-1} has been assigned to C-O stretching and O-H bending modes of alcoholic, phenolic and carboxylic groups [32]. However, any peak at 1170 cm^{-1} associated to the stretching vibration of the hydrogen bonding P=O contained in the group P-O-C (aromatic bond) [33] could not be identified, while a strong peak at 900–1000 cm^{-1} can be assigned to P-OR ester species (for the AC-H_3PO4 sample).

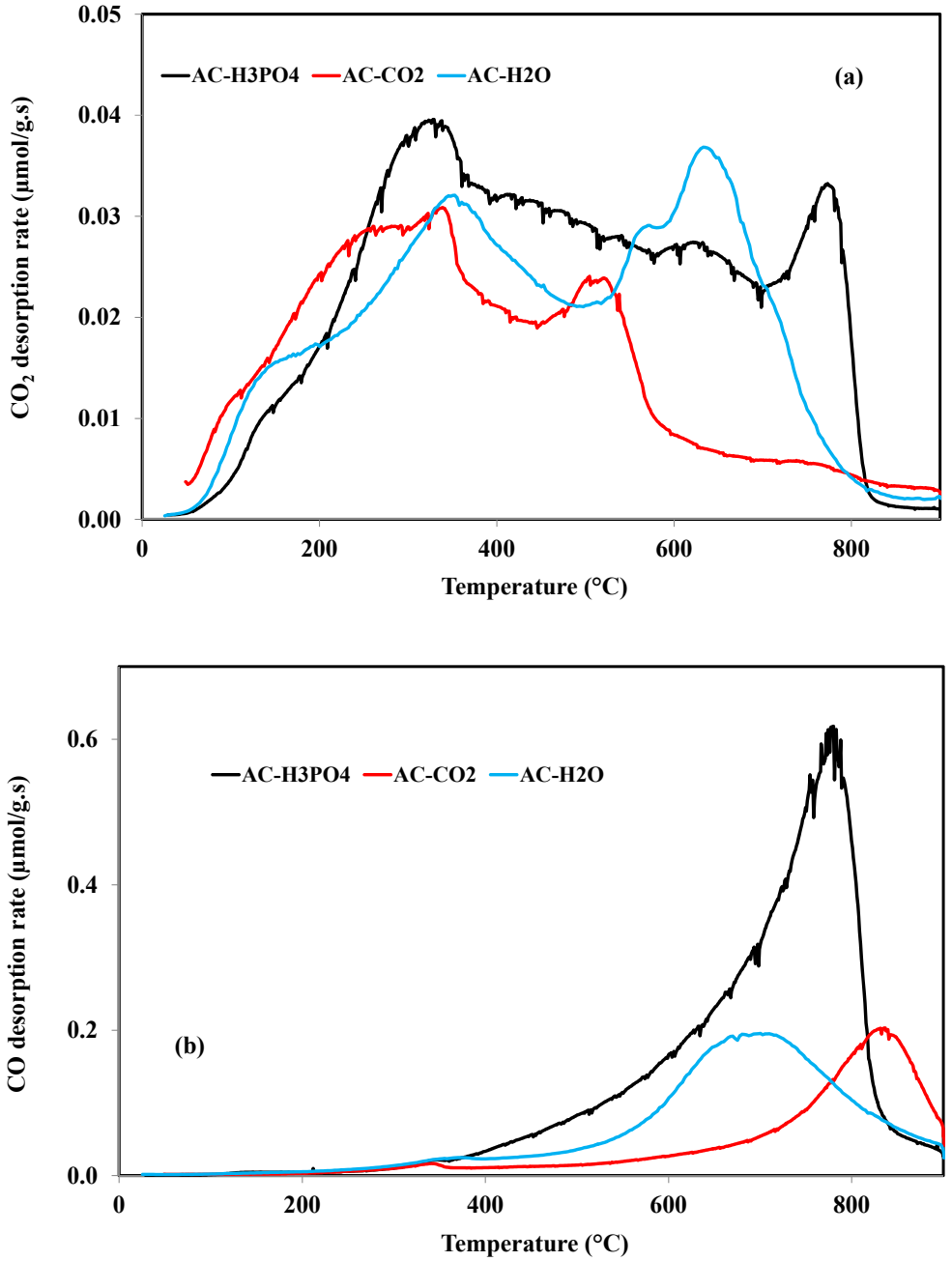

Figure 4. Desorption rates of: CO_2 (**a**); and CO (**b**) during temperature programmed desorption-mass spectroscopy (TPD-MS) of the different activated carbons.

Table 2. The cumulated amount of the emitted CO, CO_2, H_2 and H_2O during the TPD-MS analysis for the different activated carbons.

Sample	CO (mmol/g)	CO_2 (mmol/g)	H_2O (mmol/g)	H_2 (mmol/g)
AC-H_3PO_4	3.43	0.72	3.46	1.80
AC-CO_2	1.06	0.38	1.77	0.91
AC-H_2O	1.25	0.39	1.06	6.76

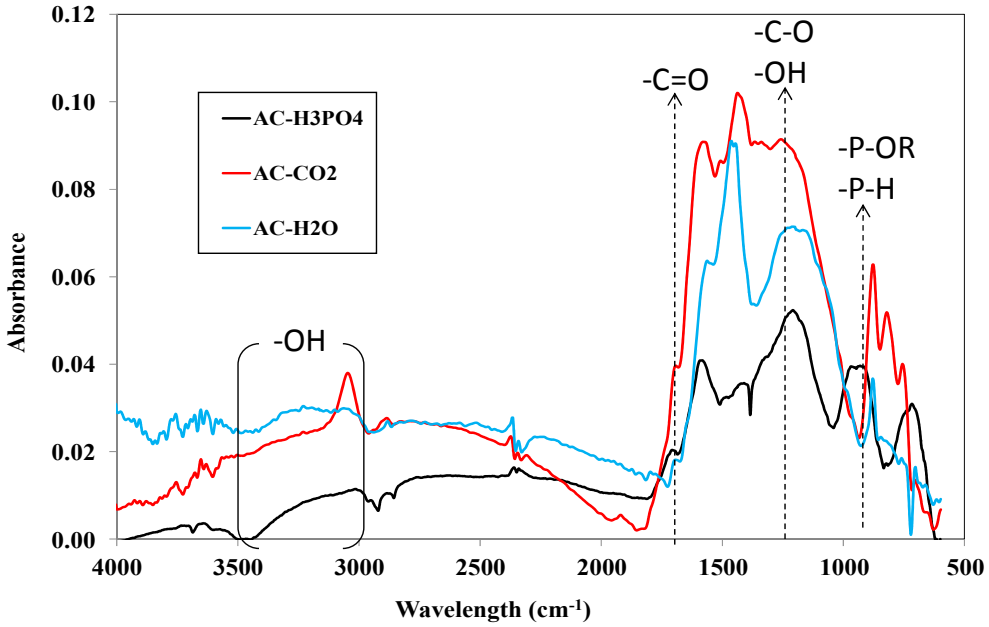

Figure 5. Fourier transform infrared spectroscopy (FTIR) spectra for the activated carbon samples.

3.2. NO_x Adsorption on the Different Activated Carbons

Figure 6 shows the breakthrough curves of NO_x through the thin sorbent layers of the three different activated carbons. The volumetric content of the sum parameter $NO_x = NO_2 + NO$ measured behind the sorbent layer is depicted in dependence of the experimental time. The inlet volumetric concentration of NO_2 was constantly kept at 5 ppm, whereas no NO was supplied. The breakthrough curves are averaged from repeated experiments with error bars indicating the standard deviation.

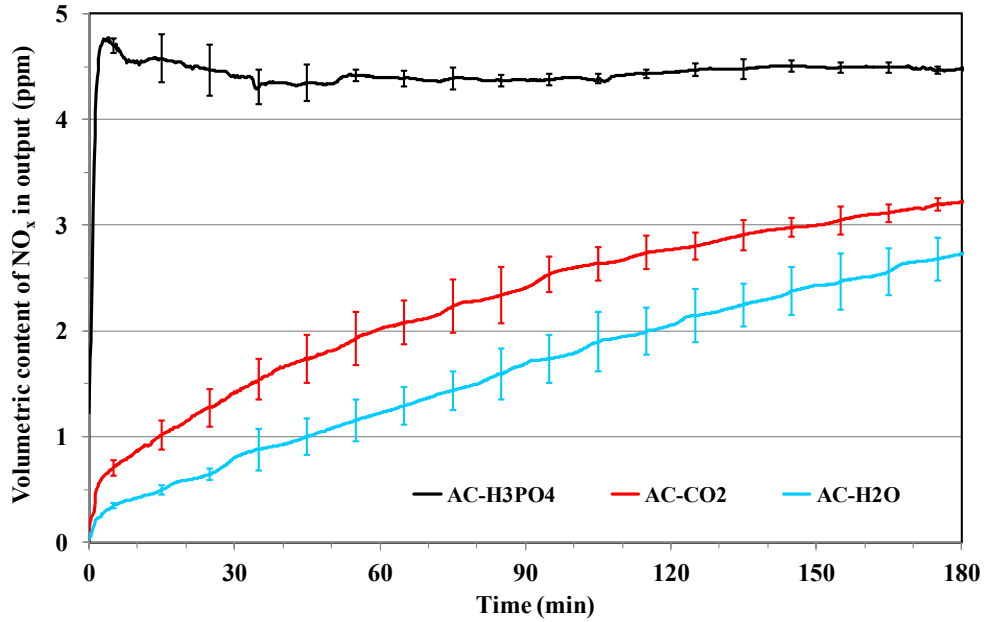

Figure 6. Breakthrough curves of NO_x through three differently activated sorbent samples made from olive stones (c_1 NO_2 = 5 ppm, c_1 NO = 0 ppm, 23 °C, 50% RH, v = 0.2 m/s, m_{Sorb} = 2 g).

As the following results show, for the assessment of the nitrogen oxide separation capacity of an activated carbon it is necessary to consider the volumetric fractions of the NO_x present downstream

the sorbent layer. Even though only NO_2 is supplied to the system, other nitrogen oxides-containing species (as NO) are formed due to reduction of NO_2 in the presence of activated carbon [11–17]. The reduction of NO_2 to NO is highly undesirable because the separation capacities of activated carbons for NO are negligible. Thus, a low activity in reducing NO_2 to NO is a desirable feature of activated carbons intended for NO_2 sorption.

For AC-CO_2 and AC-H_2O, the measured volumetric concentration of NO_x regularly increases during the experiment. AC-H_2O presents the lowest NO_x breakthrough, reaching up to the 54% of the supplied NO_2. The characteristic of the NO_x breakthrough curve of AC-H_3PO_4 is quite different. In the related experiments, in the first minutes, there is a deep increase of NO_x measured at the outlet, then a slight decline and a subsequent stabilization at 90% of the supplied NO_2. The breakthrough curves of NO and NO_2 (see Figures 7 and 8) contribute to the explanation of the results.

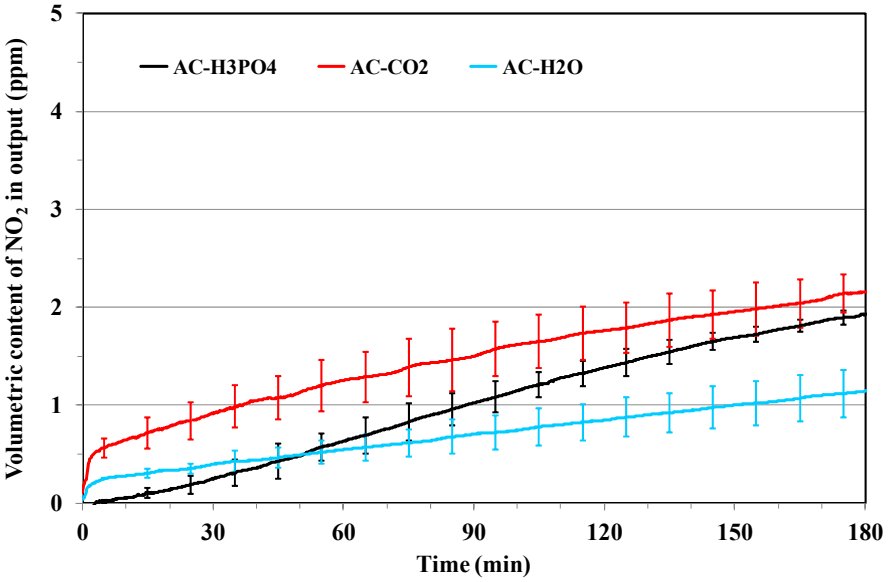

Figure 7. Breakthrough curves of NO_2 through three differently activated sorbent samples made from olive stones (c_1 NO_2 = 5 ppm, c_1 NO = 0 ppm, 23 °C, 50% RH, v = 0.2 m/s, m_{Sorb} = 2 g).

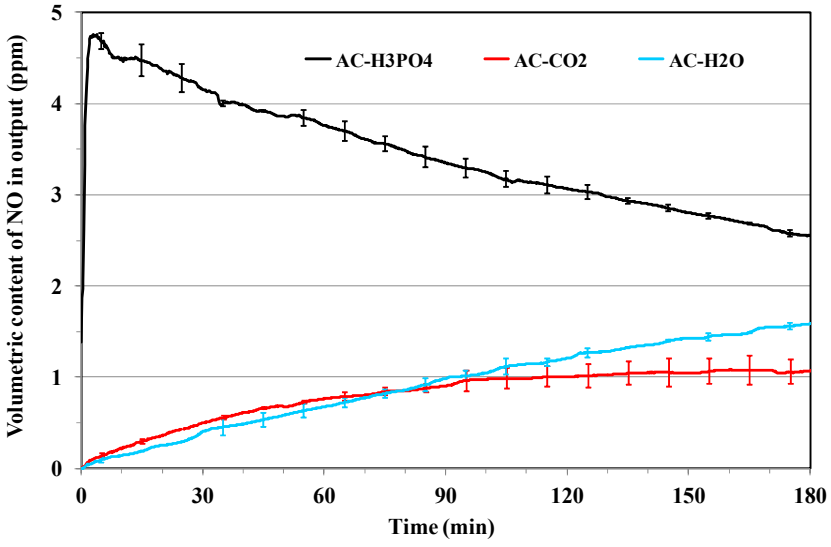

Figure 8. Breakthrough curves of NO through three differently activated sorbent samples made from olive stones (c_1 NO_2 = 5 ppm, c_1 NO = 0 ppm, 23 °C, 50% RH, v = 0.2 m/s, m_{Sorb} = 2 g).

Figure 7 show the breakthrough curves of NO_2 in the same manner as in Figure 6 for NO_x through the thin sorbent layers of the three different activated carbons. All curves increase regularly, for NO_2 the breakthrough of AC-CO_2 is the highest during the entire experimental duration of three hours. The breakthrough curves of the other two sorbents intersect after about one hour of testing. At the end of the experiment, AC-H_2O presents the lowest NO_2 breakthrough.

Figure 8 shows the measured downstream volumetric contents of NO during the experiments on the three activated carbons. At this step, it is important to mention that, in a previous study performed in similar conditions, we have shown that NO_2 is reduced to NO but no N_2 is produced during the contact between NO_2 and the different activated carbons [10,11]. For AC-CO_2 and AC-H_2O, the measured volumetric concentration of NO regularly increases during the first half of the experiment, reaching up to the 20% of the supplied concentration of NO_2 for AC-CO_2 and AC-H_2O. In the second half time of the experiments, the NO content stabilized (the curve reach a plateau) for AC-CO_2, while it continues to increase on AC-H_2O. The NO breakthrough curve of AC-H_3PO_4 is quite different. In the related experiments, at the beginning, the supplied NO_2 is almost completely and easily reduced to NO passing through the sorbent layer. During the three hours of testing, the amount of formed NO slowly decreases to reach 50% of the measured NO_2 concentration. Thus, the NO_x breakthrough characteristic of AC-H_3PO_4 shown in Figure 6 is determined by the reduction of NO_2 to NO by the sorbent.

To compare the total NO_x sorption capacities of AC-H_2O, AC-CO_2 and AC-H_3PO_4, in Figure 9, the adsorbed amounts (in g) of NO_x expressed by unit (in kg) of sorbent mass, are reported as a function of time. The mass of NO_x adsorbed (m_{ads}) is calculated using the mass balance equation reported as follows:

$$m_{ads} = \sum_{0}^{i} \frac{(M_{NO_2} \cdot \Delta y_{NO_2 i}) + (M_{NO} \cdot \Delta y_{NOi})}{V_m} \cdot \dot{V} \cdot \Delta t_i \quad (1)$$

where M_{NO2} and M_{NO} are the molar masses of NO_2 and NO, V_m the molar volume, Δy_i the difference of the volumetric content in the inlet and the outlet of the fixed-bed reactor, $\dot{V}$ the flow through the reactor and Δt_i a time interval.

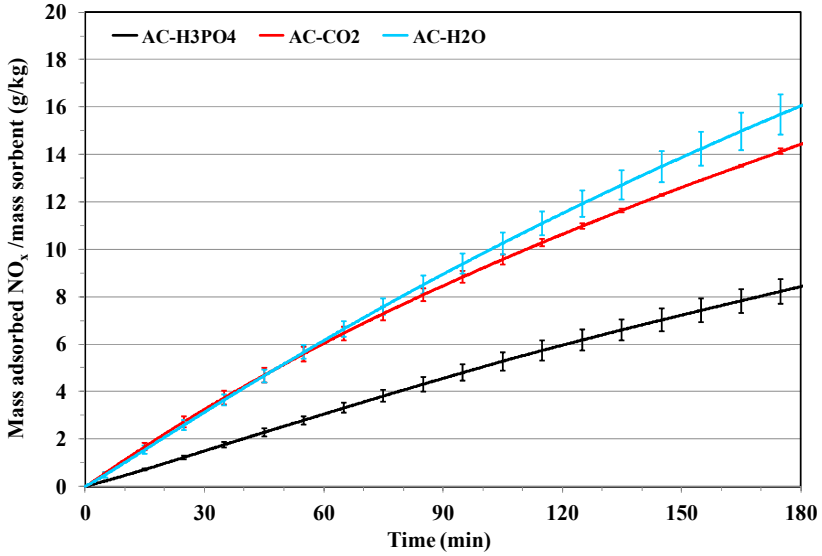

Figure 9. NO_x capacities of three differently activated sorbent samples made from olive stones loaded for 3 h with NO_2 (5 ppm) at23 °C, c_1 NO = 0 ppm,50% RH with v = 0.2 m/s.

It is apparent that AC-H_3PO_4 has the lowest total capacity, while AC-H_2O and AC-CO_2 have comparable capacities at the start of the experiment. However, at the end of the experiment, more NO_x was clearly trapped on AC-H_2O than on AC-CO_2.

The obtained capacities for NO_2 adsorption are in the same range as those available in the literature [34,35]. However, it is important to notice that the operating conditions in this present study are different from the ones available in the literature. In particular, the adsorption tests were performed at low inlet NO_2 concentrations (5 ppmv) while the ones in the literature were performed at high inlet NO_2 concentrations (500–1000 ppmv).

Effect of Porosity and Chemical Surface Groups

Porous texture and surface chemistry of activated carbons are crucial for adsorption process. However, the effect of texture parameters on NO_2 is not clearly shown in this present investigation. In fact, AC-H_3PO_4 has the highest microporous volume ($V\mu$ = 0.45 cm^3/g) and the lowest adsorption capacities (C_{NO2} = 8.4 mg/g). In contrast, AC-H_2O has the lowest microporous volume ($V\mu$ = 0.28 cm^3/g) and the highest adsorption capacities (C_{NO2} = 16 mg/g). Such results indicate that the surface chemistry plays an important role in the interaction of NO_2 with activated carbon surface. In particular, the presence of high acidic surface groups in AC-H_3PO_4 seems to inhibit the NO_2 adsorption and favoring its reduction to NO. In a previous study, it was shown that physical activation leads to the formation of basic activated carbon surfaces while chemical using phosphoric acid activation favors acid activated carbon surfaces [35]. In fact, Boehm titration for AC-H_3PO_4 indicates the presence of 1.45 mmol/g of carboxylic groups and 0.70 mmol/g of phenol groups [22]. In contrast, the basic character of activated carbons favors the NO_2 adsorption since the total basicity of AC-H_2O was equal to 1.86 mmol/g and the pHzc was equal to 10.8. Such role of basic groups could be confirmed through the comparison of the AC-CO_2 and AC-H_2O performances. In fact, these activated carbons have quite similar textural properties but the adsorption capacity for AC-H_2O (C_{NO2} = 16 mg/g) is slightly higher than AC-CO_2 (C_{NO2} = 14.4 mg/g). This difference is attributed to a higher amount of basic groups for AC-H_2O, as shown in the TPD-MS analysis. The role of surface chemistry on the interaction of NO_2 with activated carbons was already mentioned in previous investigations performed at higher NO_2 concentration (1000 ppm) [34–37]. However, no clear role of acidic and basic groups on the NO_2 adsorption capacity was identified.

To further clarify the role of the surface species towards NO_2 adsorption, FTIR analysis of the three samples before and after NO_2 adsorption were performed. Unfortunately, no evidence of N-containing species (generally detectable in the 1190–1600 cm^{-1} range) has been found for any of the sample. In any case it is interesting to observe that for the AC-H_2O and AC-CO_2 samples, that are those presenting the higher NO_2 adsorption capacity, the peaks related to C=O groups (ketones and quinones, at around 1500 cm^{-1}) and the -C-OH phenolic groups (at around 1000 cm^{-1}) disappear after adsorption of NO_2 (see FTIR spectra of AC-CO2 in Figure 10, reported as example). This behavior suggests the interaction of NO_2 with the surface oxygen groups as following:

$$-C(O) + NO_2 \rightarrow -C(ONO_2)$$

The formation of -C(ONO_2) complexes is in agreement with the TPD performed in previous investigations after NO_2 adsorption on different AC. In fact, during TPD, the NO_2 and CO molecules always desorb at the same time, as well as the CO_2 and NO molecules, thus confirming the formation of a -C(ONO_2) surface complex [6]. This complex species can be formed on carbon presenting active sites (O-containing surface groups) with only one oxygen atom, such as those that indeed disappear in the FTIR spectra after adsorption test.

Another explanation can be the difference of textural properties between the different activated carbons. At the beginning of the adsorption process, the entire surface of the AC is accessible, thus the reduction process can be limited by external surface and the chemistry of the different AC (more important for AC-H_3PO_4 and similar for the others). The only difference between AC-CO_2 and AC-H_2O corresponds to the presence of an important mesoporosity for the AC-H_2O sample. Then, the accessibility of the adsorption sites (for NO_2) is higher for AC-H_2O than for AC-CO_2,

which may explain the difference of the breakthrough curves obtained for these two adsorbents. The reduction activity may be correlated to the external surface of the AC while the adsorption of NO_2 is more dependent on the diffusion process and the basic site concentration at the surface of the AC. We can also make the hypothesis that the kinetic of NO_2 reduction is faster than the adsorption process, or energetically favorable. Of course, this comment needs to be verified and validated by further experiments.

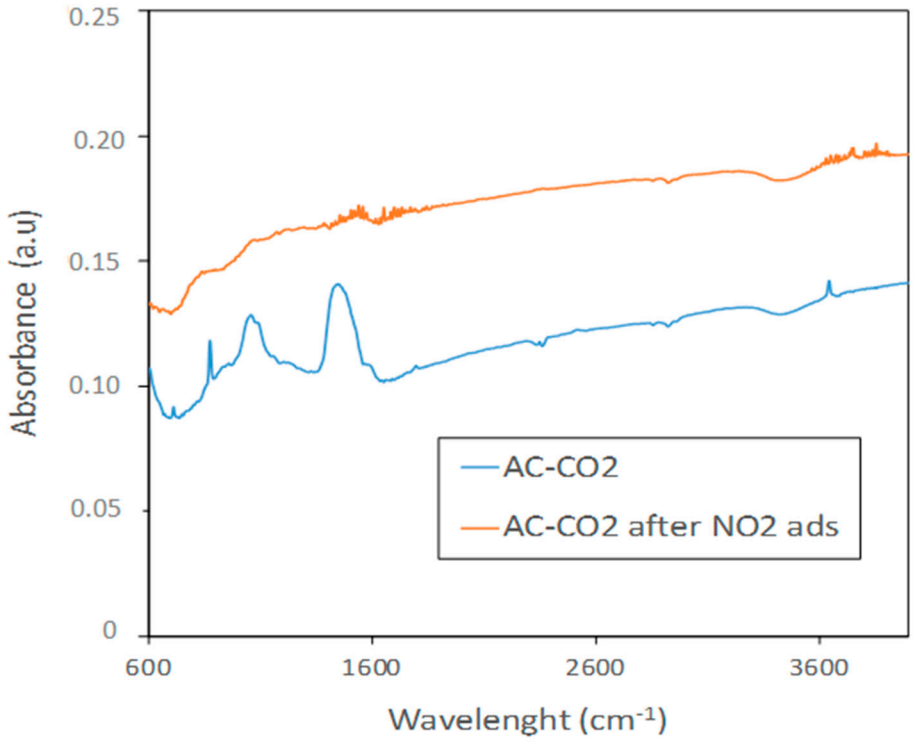

Figure 10. FTIR spectra of the AC-CO_2 sample before and after NO_2 adsorption.

4. Conclusions

In the present study, the importance of textural and surface properties of three different activated carbons is studied during the adsorption of NO_2 at room temperature and very low concentration. The results obtained during the different experiments indicate that both of these properties are responsible of NO_2 uptake and reduction to NO. The reduction rate of NO_2 is found to be very high when the activated carbon is prepared by H_3PO_4 activation. The presence of an important concentration of reducing groups at the surface of this AC (mainly anhydride groups) seems to be at the origin of this behavior. The adsorption of NO_2 is attributed to the presence of basic groups, which are more present when activation is carried out by a physical way. As AC-H_2O presents a higher amount of basic groups in comparison to AC-CO_2, its adsorption capacity is higher. The difference observed for the breakthrough curve of NO_2 for AC-CO_2 and AC-H_2O is explained by the mesoporous structure of the AC-H_2O sample, which enables a better diffusion of NO_2 inside the activated carbon particles. This study is original because it is the only work that has been published on the adsorption of NO_2 on AC (produced from a biomass) at low concentration and room temperature. These results are very interesting from a mechanistic and reactivity point of view. From our knowledge, there is no study that relates the reactivity between NO_2 and the surface of an AC. Even if all the assumptions that have been done need to be verified and confirmed by further experimentations, this work enables a better understanding of NO_2 adsorption on biomass derived sorbents. The results can be used to choose more adapted biomasses as well as to tailor the surface properties of the sorbents as a function of their potential use (reduction catalyst, adsorbent, etc.). The next step of this work will be to investigate the

form of the adsorbed species at the surface of the AC-H_2O by XPS and in situ DRIFTS experiments. Then, adsorption mechanisms could be approached.

Acknowledgments: The authors would like to thank the German Federal Ministry of Economics and Technology for financial support within the agenda for the promotion of industrial cooperative research and development (IGF) based on a decision of the German Bundestag. The access was opened by the IUTA e. V., Duisburg, and organized by the AiF (IGF-Project Nos. 14883 and 15751).

Author Contributions: All authors contributed equally to the work done.

Conflicts of Interest: The authors declare no conflict of interest.

References

1. Wilkins, C.K.; Clausen, P.A.; Wolkoff, P.; Larsen, S.T.; Hammer, M.; Larsen, K.; Hansen, V.; Nielsen, G.D. Formation of strong airway irritants in mixtures of isoprene/ozone and isoprene/ozone/nitrogen dioxide. *Environ. Health Perspect.* **2001**, *109*, 937–941. [CrossRef] [PubMed]
2. Blondeau, P.; Iordache, V.; Poupard, O.; Genin, D.; Allard, F. Relationship between outdoor and indoor air quality in eight French schools. *Indoor Air* **2005**, *15*, 2–12. [CrossRef] [PubMed]
3. Gou, X.; Wu, C.; Zhang, K.; Xu, G.; Si, M.; Wang, Y.; Wang, E.; Liu, L.; Wu, J. Low Temperature Performance of Selective Catalytic Reduction of NO with NH3 under a Concentrated CO_2 Atmosphere. *Energies* **2015**, *8*, 12331–12341. [CrossRef]
4. Levasseur, B.; Ebrahim, A.M.; Burress, J.; Bandosz, T.J. Interactions of NO_2 at ambient temperature with cerium–zirconium mixed oxides supported on SBA-15. *J. Hazard. Mater.* **2011**, *197*, 294–303. [CrossRef] [PubMed]
5. Hodjati, S.; Vaezzadeh, K.; Petit, C.; Pitchon, V.; Kiennemann, A. Absorption/desorption of NO_x process on perovskites: Performances to remove NO_x from a lean exhaust gas. *Appl. Catal. B Environ.* **2000**, *26*, 5–16. [CrossRef]
6. Jeguirim, M.; Tschamber, V.; Brilhac, J.F.; Ehrburger, P. Interaction mechanism of NO_2 with carbon black: Effect of surface oxygen complexes. *J. Anal. Appl. Pyrolysis* **2004**, *72*, 171–181. [CrossRef]
7. Nowicki, P.; Pietrzak, R.; Wachowska, H. Sorption properties of active carbons obtained from walnut shells by chemical and physical activation. *Catal. Today* **2010**, *150*, 107–114. [CrossRef]
8. Pietrzak, R. Sawdust pellets from coniferous species as adsorbents for NO_2 removal. *Bioresour. Technol.* **2010**, *101*, 907–913. [CrossRef] [PubMed]
9. Belala, Z.; Belhachemi, M.; Jeguirim, M. Activated Carbon Prepared from Date Pits for the Retention of NO_2 at Low Temperature. *Int. J. Chem. React. Eng.* **2014**, *12*, 717–726. [CrossRef]
10. Ghouma, I.; Jeguirim, M.; Dorge, S.; Limousy, L.; Matei Ghimbeu, C.; Ouederni, A. Activated carbon prepared by physical activation of olive stones for the removal of NO_2 at ambient temperature. *C. R. Chim.* **2015**, *18*, 63–74. [CrossRef]
11. Belhachemi, M.; Jeguirim, M.; Limousy, L.; Addoun, F. Comparison of NO_2 removal using date pits activated carbon and modified commercialized activated carbon via different preparation methods: Effect of porosity and surface chemistry. *Chem. Eng. J.* **2014**, *253*, 121–129. [CrossRef]
12. Heschel, W.; Ahnert, F. Multicomponent adsorption of NO_2, SO_2 and butane from air on activated carbon. *Adsorpt. Sci. Technol.* **2002**, *20*, 353–370.
13. Labaki, M.; Issa, M.; Smeekens, S.; Heylen, S.; Kirschhock, C.E.A.; Villani, K.; Jeguirim, M.; Habermacher, D.; Brilhac, J.F.; Martens, J.A. Modeling of NO_x adsorption–desorption–reduction cycles on a ruthenium loaded Na–Y zeolite. *Appl. Catal. B Environ.* **2010**, *97*, 13–20. [CrossRef]
14. Zouaoui, N.; Labaki, M.; Jeguirim, M. Diesel soot oxidation by nitrogen dioxide, oxygen and water under engine exhaust conditions: Kinetics data related to the reaction mechanism. *C. R. Chim.* **2014**, *17*, 672–680. [CrossRef]
15. Bennici, S.; Gervasini, A.; Ravasio, N.; Zaccheria, F. Optimization of Tailoring of CuO_x Species of Silica Alumina Supported Catalysts for the Selective Catalytic Reduction of NO_x. *J. Phys. Chem. B* **2003**, *107*, 5168–5176. [CrossRef]
16. Limousy, L.; Mahzoul, H.; Brilhac, J.F.; Gilot, P.; Garin, F.; Maire, G. SO_2 sorption on fresh and aged SO_x traps. *Appl. Catal. B Environ.* **2003**, *42*, 237–249. [CrossRef]

17. Sager, U.; Schmidt, F. Adsorption of Nitrogen Oxides, Water Vapour and Ozone onto Activated Carbon. *Adsorpt. Sci. Technol.* **2009**, *27*, 135–145. [CrossRef]
18. Sager, U.; Suhartiningsih; Schmidt, F. Einfluss der NO2-Dosierung auf Adsorptionsfiltertests. *Chem. Ing. Tech.* **2010**, *82*, 1737–1742. [CrossRef]
19. Sager, U.; Schmidt, W.; Schmidt, F. Suhartiningsih Catalytic reduction of nitrogen oxides via nanoscopic oxide catalysts within activated carbons at room temperature. *Adsorption* **2013**, *19*, 1027–1033. [CrossRef]
20. Sager, U.; Däuber, E.; Asbach, C.; Bathen, D.; Schmidt, F.; Weidenthaler, C.; Tseng, J.C.; Schmidt, W. Differences between the adsorption of NO_2 and NO on modified activated carbon/Unterschiede bei der Adsorption von NO_2 und NO an modifizierter Aktivkohle. *Air Qual. Control* **2014**, *74*, 181–184.
21. Sager, U.; Däuber, E.; Bathen, D.; Asbach, C.; Schmidt, F.; Tseng, J.-C.; Pommerin, A.; Weidenthaler, C.; Schmidt, W. Influence of the degree of infiltration of modified activated carbons with CuO/ZnO on the separation of NO_2 at ambient temperatures. *Adsorpt. Sci. Technol.* **2016**, *34*, 307–319. [CrossRef]
22. Limousy, L.; Ghouma, I.; Ouederni, A.; Jeguirim, M. Amoxicillin removal from aqueous solution using activated carbon prepared by chemical activation of olive stone. *Environ. Sci. Pollut. Res.* **2017**, *24*, 9993–10004. [CrossRef] [PubMed]
23. Travis, W.; Gadipelli, S.; Guo, Z. Superior CO_2 adsorption from waste coffee ground derived carbons. *RSC Adv.* **2015**, *5*, 29558–29562. [CrossRef]
24. Jagtoyen, M.; Derbyshire, F. Activated carbons from yellow poplar and white oak by H3PO4 activation. *Carbon* **1998**, *36*, 1085–1097. [CrossRef]
25. Srinivas, G.; Krungleviciute, V.; Guo, Z.-X.; Yildirim, T. Exceptional CO_2 capture in a hierarchically porous carbon with simultaneous high surface area and pore volume. *Energy Environ. Sci.* **2013**, *7*, 335–342. [CrossRef]
26. Srinivas, G.; Burress, J.; Yildirim, T. Graphene oxide derived carbons (GODCs): Synthesis and gas adsorption properties. *Energy Environ. Sci.* **2012**, *5*, 6453–6459. [CrossRef]
27. Román, S.; Ledesma, B.; Álvarez-Murillo, A.; Al-Kassir, A.; Yusaf, T. Dependence of the Microporosity of Activated Carbons on the Lignocellulosic Composition of the Precursors. *Energies* **2017**, *10*, 542. [CrossRef]
28. Guizani, C.; Jeguirim, M.; Gadiou, R.; Escudero Sanz, F.J.; Salvador, S. Biomass char gasification by H_2O, CO_2 and their mixture: Evolution of chemical, textural and structural properties of the chars. *Energy* **2016**, *112*, 133–145. [CrossRef]
29. Figueiredo, J.L.; Pereira, M.F.R.; Freitas, M.M.A.; Órfão, J.J.M. Modification of the surface chemistry of activated carbons. *Carbon* **1999**, *37*, 1379–1389. [CrossRef]
30. Reddy, K.S.K.; Al Shoaibi, A.; Srinivasakannan, C. A comparison of microstructure and adsorption characteristics of activated carbons by CO_2 and H_3PO_4 activation from date palm pits. *New Carbon Mater.* **2012**, *27*, 344–351. [CrossRef]
31. El-Hendawy, A.-N.A. Influence of HNO_3 oxidation on the structure and adsorptive properties of corncob-based activated carbon. *Carbon* **2003**, *41*, 713–722. [CrossRef]
32. Shen, W.; Li, Z.; Liu, Y. Surface chemical functional groups modification of porous carbon. *Recent Pat. Chem. Eng.* **2008**, *1*, 27–40. [CrossRef]
33. Puziy, A.M.; Poddubnaya, O.I.; Martínez-Alonso, A.; Suárez-García, F.; Tascón, J.M.D. Synthetic carbons activated with phosphoric acid: I. Surface chemistry and ion binding properties. *Carbon* **2002**, *40*, 1493–1505. [CrossRef]
34. Nowicki, P.; Skibiszewska, P.; Pietrzak, R. NO_2 removal on adsorbents prepared from coffee industry waste materials. *Adsorption* **2013**, *19*, 521–528. [CrossRef]
35. Nowicki, P.; Wachowska, H.; Pietrzak, R. Active carbons prepared by chemical activation of plum stones and their application in removal of NO_2. *J. Hazard. Mater.* **2010**, *181*, 1088–1094. [CrossRef] [PubMed]
36. Nowicki, P.; Pietrzak, R. Carbonaceous adsorbents prepared by physical activation of pine sawdust and their application for removal of NO_2 in dry and wet conditions. *Bioresour. Technol.* **2010**, *101*, 5802–5807. [CrossRef] [PubMed]
37. Gadipelli, S.; Guo, Z.X. Graphene-based materials: Synthesis and gas sorption, storage and separation. *Prog. Mater. Sci.* **2015**, *69*, 1–60. [CrossRef]